TECHNICAL REPORT 1844
November 2000

Parametric Study of Propagation in Evaporation Ducting and Subrefractive Conditions

R. A. Paulus

SSC San Diego
San Diego, CA 92152–5001

REPORT DOCUMENTATION PAGE

1. REPORT DATE (DD-MM-YYYY)	2. REPORT TYPE	3. DATES COVERED (FROM - TO)
01-11-2000	Technical Report	xx-xx-2000 to xx-xx-2000

4. TITLE AND SUBTITLE	5a. CONTRACT NUMBER
Parametric Study of Propagation in Evaporation Ducting and Subrefractive Conditions	5b. GRANT NUMBER
	5c. PROGRAM ELEMENT NUMBER
Unclassified	

6. AUTHOR(S)	5d. PROJECT NUMBER
Paulus, R. A. ;	5e. TASK NUMBER
	5f. WORK UNIT NUMBER

7. PERFORMING ORGANIZATION NAME AND ADDRESS	8. PERFORMING ORGANIZATION REPORT NUMBER
SPAWAR Systems Center San Diego SSC San Diego San Diego , CA 92152-5001	

9. SPONSORING/MONITORING AGENCY NAME AND ADDRESS	10. SPONSOR/MONITOR'S ACRONYM(S)
,	11. SPONSOR/MONITOR'S REPORT NUMBER(S)

12. DISTRIBUTION/AVAILABILITY STATEMENT

A
PUBLIC RELEASE

,

13. SUPPLEMENTARY NOTES

14. ABSTRACT

This report quantifies propagation loss differences that result from approximating the full stability-dependent refractivity profiles with neutral-stability profiles parameterized by duct height. It also develops a parameterization for subrefractive profiles and quantifies the propagation loss differences that result from approximating the full stability-dependent refractivity profiles with neutral-stability profiles parameterized by subrefractive layer height.

15. SUBJECT TERMS

16. SECURITY CLASSIFICATION OF:			**17. LIMITATION OF ABSTRACT**	**18. NUMBER OF PAGES**	**19a. NAME OF RESPONSIBLE PERSON**
			Public Release	43	Fenster, Lynn lfenster@dtic.mil
a. REPORT Unclassified	**b. ABSTRACT** Unclassified	**c. THIS PAGE** Unclassified			**19b. TELEPHONE NUMBER** **International Area Code** **Area Code Telephone Number** 703 737-9007 **DSN** 427-9007

SSC SAN DIEGO
San Diego, California 92152-5001

Ernest L. Valdes, CAPT, USN
Commanding Officer

R. C. Kolb
Executive Director

ADMINISTRATIVE INFORMATION

The work described in this report was prepared for the Office of Naval Research (ONR 322) by the SSC San Diego Atmospheric Propagation Branch (D858).

Released by
R. A. Paulus, Head
Atmospheric Propagation Branch

Under authority of
C. J. Sayre, Head
Electromagnetics &
Advanced Technology
Division

SB

EXECUTIVE SUMMARY

The refractive structure of the marine atmospheric surface layer at microwave frequencies can be characterized by a parameter called the “evaporation duct height,” which is the height of the minimum in the profile of the modified refractivity. Using bulk measurements of air temperature, relative humidity, wind speed, and sea surface temperature, scientists can calculate profiles of meteorological variables in the surface layer with well-known flux profile relationships. The National Climatic Data Center Asheville maintains a database of these measurements from ocean weather stations and ships of opportunity. A set of data recorded from 1970 to 1984 was used to construct an evaporation duct height climatology. This climatology has been used successfully to statistically model evaporation duct propagation and frequency diversity effects in the open ocean. These models were developed on the assumption that propagation losses represented by a neutral-stability profile are not significantly different from the full, stability-dependent profile for common departures from neutrality. A recent study showed similar success, with some qualifications, in the littoral. This latter study concluded that the evaporation duct climatology could be improved by adding statistics for subrefraction in the surface layer.

An equation for modified refractivity parametric in subrefractive layer height is developed. Then, the differences in propagation loss resulting from approximating the full stability-dependent refractivity profiles with neutral-stability profiles parameterized by the characteristic height are quantified for typical low-altitude propagation scenarios. Parametric variation of the bulk meteorological parameters includes the following:

- Wind speed over the range of 2.5 to 10 m/s in increments of 2.5 m/s,
- Sea temperature over the range of 5 to 30°C in increments of 5°C,
- Air temperatures over the range of 5°C less than sea temperature to 3°C greater than sea temperature in increments of 0.5°C,
- Relative humidity over the range of 60 to 100% in increments of 5%.

Pressure and reference measurement heights were held constant at 1000 mb and 10 m msl. This variation resulted in 3,178 valid surface layer refractivity profiles, of which 3,039 were ducting and 139 were subrefractive. The resulting differences in propagation loss are statistically described.

CONTENTS

Figures

Tables

INTRODUCTION

This report quantifies propagation loss differences that result from approximating the full stability-dependent refractivity profiles with neutral-stability profiles parameterized by duct height. It also develops a parameterization for subrefractive profiles and quantifies the propagation loss differences that result from approximating the full stability-dependent refractivity profiles with neutral-stability profiles parameterized by subrefractive layer height.

BACKGROUND

The refractive structure of the marine atmospheric surface layer at microwave frequencies can be characterized by a parameter called the "evaporation duct height," which is the height of the minimum in the profile of the modified refractivity. Using bulk measurements of air temperature, relative humidity, wind speed, and sea surface temperature, scientists can calculate profiles of meteorological variables in the surface layer with well-known flux profile relationships. The National Climatic Data Center Asheville maintains a database of these measurements from ocean weather stations and ships of opportunity. A set of data recorded from 1970 to 1984 was used to construct an evaporation duct height climatology (Anderson, 1987; Patterson, 1987). The evaporation duct height can be used to reconstruct a modified refractivty profile and applied to propagation problems under the assumption that the propagation losses represented by a neutral-stability profile are not significantly different from the full stability-dependent profile for common departures from neutrality. The evaporation duct height climatology has been used successfully to statistically model evaporation duct propagation (Hitney and Vieth, 1990) and frequency diversity effects (Hitney and Hitney, 1990) in the open ocean and, with some qualification, in the littoral (Paulus and Anderson, 2000). Paulus and Anderson (2000) concluded that the evaporation duct climatology could be improved by adding statistics for subrefraction in the surface layer.

The DATA AND MODELS section reviews the development of the equation for modified refractivity parametric in duct height for neutral stability and extends this parameterization to account for subrefraction by subrefractive layer height and "negative evaporation duct height." The model of the marine atmospheric surface layer is described and the parametric variations of the surface layer model input data are defined. The electromagnetic propagation model is described and the propagation model output data selected for analysis are defined. The RESULTS section presents the statistics and case studies. The CONCLUSIONS section summarizes the findings of this work.

DATA AND MODELS

REFRACTIVITY CHARACTERIZATION

The refractive index, n, of the atmosphere is often expressed in terms of refractivity, $N = (n\text{-}1) \times 10^6$, or modified refractivity, $M = N + 0.157z$, where z is height in meters. Refractivity can be measured directly with a refractometer or derived from measurements of pressure, P (mb), temperature, T (K), and water vapor pressure, e (mb), using

$$N = \frac{77.6P}{T} + 3.73\times10^5 \frac{e}{T^2}. \tag{1}$$

Refractivity is normally a decreasing function with altitude whereas modified refractivity is normally an increasing function with altitude.

In parametric studies of evaporation duct propagation, it is convenient to have an equation for the modified refractivity profile as a function of height and evaporation duct height. In the atmospheric surface layer, potential refractivity,

$$N_p = \frac{77.6P_0}{\theta} + 3.73\times10^5 \frac{e_p}{\theta^2}, \tag{2}$$

is a convenient parameter because of its conservative property in a dynamic atmosphere. Here, θ is potential temperature (°K), e_p is potential water vapor pressure (mb), and P_0 is a reference pressure level (taken to be 1000 mb). Panofsky and Dutton (1984) provide a general expression for the gradient of a conservative scalar in the atmospheric surface layer which, for potential refractivity, becomes

$$\frac{\partial N_p}{\partial z} = \frac{N_{p^*}}{\kappa z}\phi\left(\frac{z}{L}\right), \tag{3}$$

where z is altitude, N_{p*} is the potential refractivity scaling parameter, κ is von Karman's constant, φ is a stability function, and L is the Monin Obukhov stability length. For neutral stability, φ is 1 and integrating equation (3) from a lower limit of z_0 yields

$$N_p(z) - N_p(z_0) = \frac{N_{p^*}}{\kappa}\ln\frac{z}{z_0}, \tag{4}$$

where the aerodynamic roughness length, z_0, is taken to be 1.5 x 10^{-4} m.

From geometric optics, the critical gradient required for trapping is that which yields a ray curvature equal to the earth's curvature (Bean and Dutton, 1968):

$$\frac{dN}{dz} = -\frac{10^6}{a} = -0.157 \quad \text{N/m}, \tag{5}$$

where a is the earth radius in meters. In terms of modified refractivity, the critical gradient is

$$\frac{dM}{dz} = 0. \tag{6}$$

That is, the evaporation duct height is the top of the surface trapping layer. Gossard and Strauch (1983) relate N_p to N and M by

$$N_p = N + 0.024z \text{ and} \tag{7}$$

$$N_p = M - 0.13z \tag{8}$$

so that $dN_p/dz = -0.13$ for trapping. Defining the height at which this critical gradient occurs as the evaporation duct height, δ, equation (3) becomes

$$-0.13 = \frac{N_{p^*}}{\kappa\delta}. \tag{9}$$

Solving equation (4) for N_{p*}, substituting in equation (9), and using the relation of equation (8) yields

$$M(z) = M_0 + 0.13z - 0.13\delta \ln\left(\frac{z}{z_0}\right), \tag{10}$$

where M_0, the value of modified refractivity at the sea surface temperature assuming saturation, approximates $M(z_0)$. Similarly, it would be convenient to have an equation for the modified refractivity profile as a function of height and some parameterization of subrefraction. Similar to the height of the evaporation duct being the top of a surface trapping layer where $dM/dz = 0$, there is a height that is the top of a surface subrefractive layer where $dN/dz = 0$. Defining the height at which this critical gradient occurs as the subrefractive layer height, ς, $dN_p/dz = 0.024$ and equation (9) becomes

$$0.024 = \frac{N_{p^*}}{\kappa\varsigma}. \tag{11}$$

Again, solving equation (4) for N_{p*}, substituting in equation (11), and using the relation of equation (8) yields

$$M(z) = M_0 + 0.13z + 0.024\varsigma \ln\left(\frac{z}{z_0}\right). \tag{12}$$

Equations (10) and (12) can generate ducting and subrefractive profiles parametric in evaporation duct height and subrefractive layer height, respectively. Jeske (1973) referred to subrefraction as an "anti-duct." In his formulation, subrefractive conditions produced a negative duct height. While a negative duct height is not physically realistic, that parameter does allow one to analyze results of all refractive conditions versus one parameter. Simultaneous solution of equations (10) and (12) produces

$$\delta = -0.185\varsigma\,, \tag{13}$$

which can be used to present results against whichever parameterization is more convenient. For input to the propagation model, the modified refractivity profile was digitized at discrete heights in meters according to

$$z = e^{x}, \tag{14}$$

where x = -2 to 5 in 0.5 increments, *i.e.*, 0.1354 to 148.4132 m.

SURFACE LAYER MODEL

The surface layer model developed by Frederickson, Davidson, and Goroch (2000) was used for this study. Model input requirements are wind speed (m/s), air temperature (°C), sea surface temperature (°C), relative humidity (%), atmospheric pressure (mb), and the heights of measurement of the four atmospheric parameters (m msl). Table 1 shows valid values of these input parameters. Model outputs are the evaporation duct height (0 to 50 m) and the profile of modified refractivity from the sea surface to 50 m msl. In some very stable cases, the model algorithm will not converge and there is no valid solution for some combinations of input data.

Table 1. Surface layer model input parameter limits.

Parameter	Inclusive Limits
Wind speed	1 to 40 m/s
Air temperature	-55 to 55°C
Sea surface temperature	-2 to 40°C
Relative humidity	0 to 101%
Atmospheric pressure	940 to 1040 mb
Measurement height	1 to 50 m

For our purposes, refractivity profiles, *N(z)*, were computed along with the modified refractivity profiles for the subrefractive conditions. The height of the maximum value of refractivity was selected as the subrefractive layer height. For the comparisons in this report, we used only evaporation duct heights and subrefractive layer heights <50 m. The Monin–Obukhov length, L, was also extracted from the surface layer model to generate the stability parameter, z/L.

METEOROLOGICAL PARAMETERS

The variation of the bulk parameters was arbitrarily selected to be typical ocean conditions by examination of the climatological data from the Marine Climatic Atlas of the World series (U.S. Navy, 1974). The data presented in the climatology are independent. There is no information as to the joint occurrence probability of any combination of the meteorological parameters. Here, we have assumed each combination of bulk parameters is equally probable. Table 2 shows the input data range and the increment used for iteration. This combination produces a potential for 3,672 different environmental conditions. However, 281 conditions had evaporation duct heights equal to or greater than 50 m, 209 had subrefractive layer heights equal to or greater than 50 m, and in four cases, the surface layer algorithm did not converge to a result. Thus, there were 3,178 environments for which propagation loss could be calculated. Of these, 3,039 (96%) were ducting conditions and 139 were subrefractive (4%) conditions. Of the ducting conditions, 635 were stable ducts (20%) and 2,404 were unstable ducts (76%)

Table 2. Bulk parameter variations.

Parameter	Inclusive Limits	Increment
Wind speed	2.5 to 10 m/s	2.5 m/s
Air temperature	Sea - 5 to Sea +3°C	0.5°C
Sea surface temperature	5 to 30°C	5°C
Relative humidity	60 to 100%	5%
Atmospheric pressure	1000 mb	None
Measurement height	10 m	None

Figure 1 shows the statistics and histogram for the simulated evaporation duct heights. This figure indicates good coverage of duct heights for the simulated data. Figure 2 shows the distribution of simulated duct heights (positive duct heights only) calculated with the Frederickson et al. (2000) model plotted with the distribution of duct heights calculated using the current standard evaporation duct model (Paulus, 1989) for the same parametric data set. The shapes of the two distributions are similar except that the Frederickson distribution has a lower mean (9.27 m compared to 10.8 m) and greater kurtosis. Figure 3 shows evaporation duct height versus the z/L stability parameter that Frederickson et al. (2000) define as

$$\frac{z}{L} = \frac{z\kappa g\theta_{*v}}{\theta_v u_*^2}. \tag{15}$$

Here, θ_v is virtual potential temperature, θ_{*v} is the virtual potential temperature scaling parameter, and u_* is the scaling parameter for momentum. Physically, z/L is the ratio of turbulent kinetic energy generated by thermal buoyancy to turbulent kinetic energy generated by wind shear. Table 3 shows a qualitative description of z/L based on Panofsky and Dutton (1984). A wide range of stability occurs in the simulated data, with most (72%) in the range, $|z/L| < 0.5$. This range is approximately the near-neutral Pasquill–Gifford stability category D (Hsu, 1992). Notice from figure 3 that all negative duct heights (subrefractive layers) occur under stable conditions and mostly near neutral. The largest duct heights also occur under stable conditions and mostly near neutral. It is operationally significant that the greatest variation in duct heights occurs near neutral. Blanc (1987) showed that near neutral is the region in which it is most difficult to accurately determine stability using bulk measurements. Thus, errors in determining the evaporation duct characteristics are likely greatest near neutral.

Table 3. Description of z/L with respect to wind speed and air–sea temperature difference (ASTD).

Value of z/L	Description	Physical Meaning
Strongly negative ($z/L < -0.5$)	Unstable	Thermal convection dominant; lighter winds or large, negative ASTD
Negative, but small ($-0.5 < z/L < 0$)	Unstable, near neutral	Mechanical turbulence dominant; higher winds or small, negative ASTD
Zero	Neutral	Purely mechanical turbulence
Slightly positive ($0 < z/L < 0.5$)	Stable, near neutral	Mechanical turbulence slightly damped by thermal stratification; higher winds or small, positive ASTD
Strongly positive ($z/L > 0.5$)	Stable	Mechanical turbulence severely reduced by thermal stratification; lighter winds or large, positive ASTD

Minimum duct height (m)	-9.2
Maximum duct height (m)	49.4
Mean	8.76
Median	7.00
Variance	57.94
Standard Deviation	7.61
Total Observations	3178

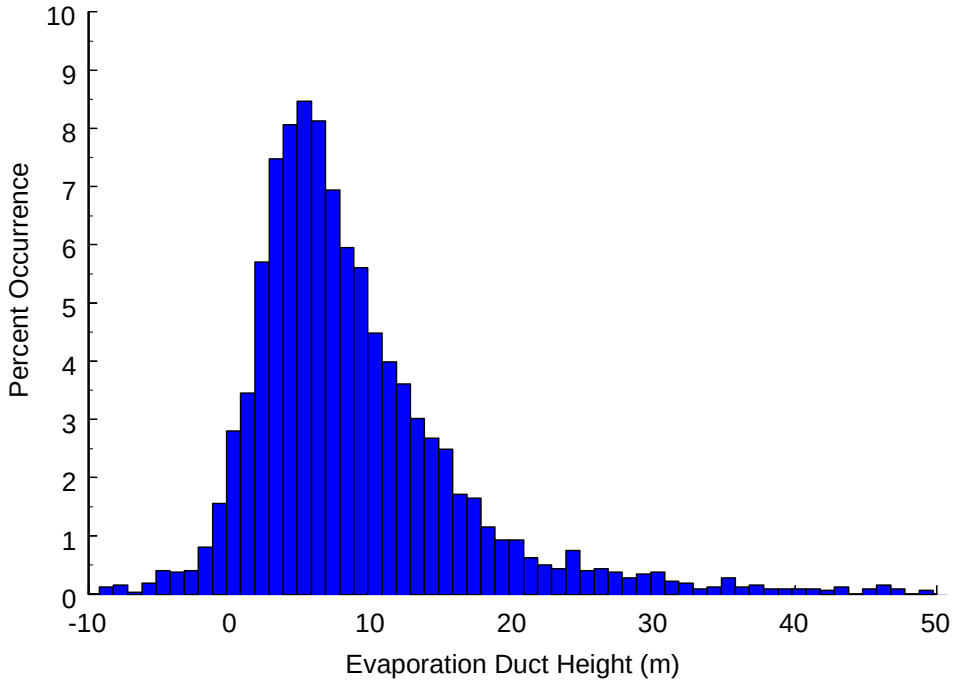

Figure 1. Statistics and histogram for computed evaporation duct heights. Histogram is in 1-m bins.

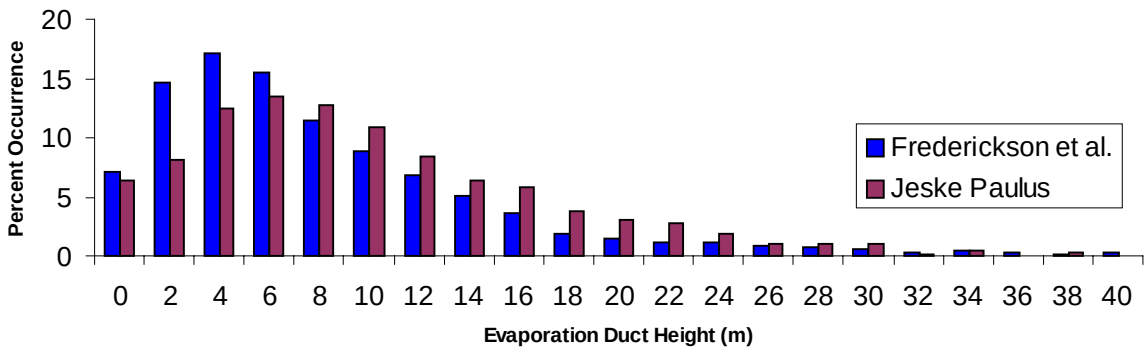

Figure 2. Comparison of the simulated evaporation duct height distributions calculated using the Frederickson et al. (2000) model and the Jeske Paulus (Paulus, 1989) model with 2-m bin size.

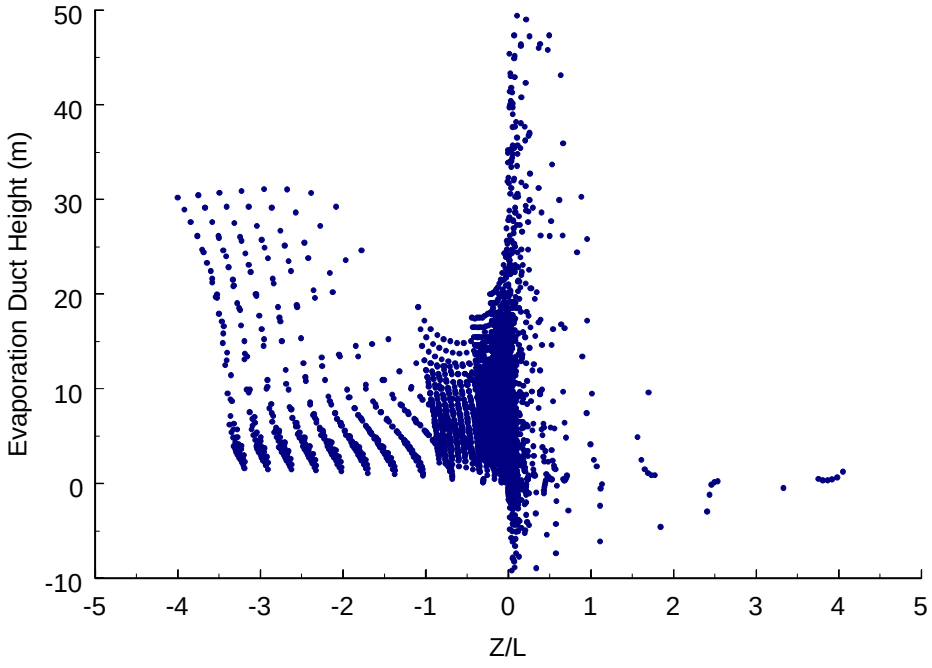

Figure 3. Evaporation duct height versus the stability parameter, z/L.

PROPAGATION MODELING

The propagation model used in this study was the hybrid ray-optics/parabolic equation Radio Physical Optics (RPO) model (Hitney, 1992). RPO can partially account for sea surface roughness by assuming a fully arisen sea for the given wind speed. However, for this study, the sea surface was assumed flat, and molecular absorption was neglected. The propagation scenarios selected used a horizontally polarized transmitter at 15 m msl with a 2° wide Gaussian beam at 0° elevation. Propagation loss values were calculated for a receiver located at 5 m msl at frequencies of 3, 5, and 9 GHz at ranges of 10, 25, and 40 km and for 18 GHz at 10 and 25 km. The 25-km range is approximately at the 4/3 earth radio horizon and the 10-km range lies well within the horizon. The 40-km range was selected such that troposcatter was not a factor in the standard atmosphere (4/3 earth radius) propagation loss. Propagation loss was calculated using the 3,178 full stability-dependent refractivity profiles and the neutral profiles using the same duct or subrefractive layer height in equation (10) or (12). The solid line in figures 4 and 5 shows standard atmosphere propagation loss at a 5-m altitude for each of the four frequencies. The vertical lines in each plot indicate the variation in propagation loss over the 3,178 profiles at each range. At 3 and 5 GHz (figure 4), evaporation ducting causes signal levels to be near or above standard. Subrefraction causes signal levels to be below standard. At 9 GHz (top graph, figure 5), evaporation ducting causes signal levels to be near or above standard at 25 and 40 km, but subrefraction and evaporation ducting reduce signal levels below standard at 10 km. Evaporation ducting causes the maximum modeled propagation loss of 141.5 dB at 10 km and subrefraction causes the maximum losses of 184.5 dB and 211.1 dB at 25 and 40 km, respectively. Evaporation ducting causing greater propagation loss within the horizon was expected, as it has been modeled (Dockery, 1987) and measured (Anderson, 1995) previously. Likewise, the propagation effects at 18 GHz (bottom graph, figure 5) are similar to those at 9 GHz.

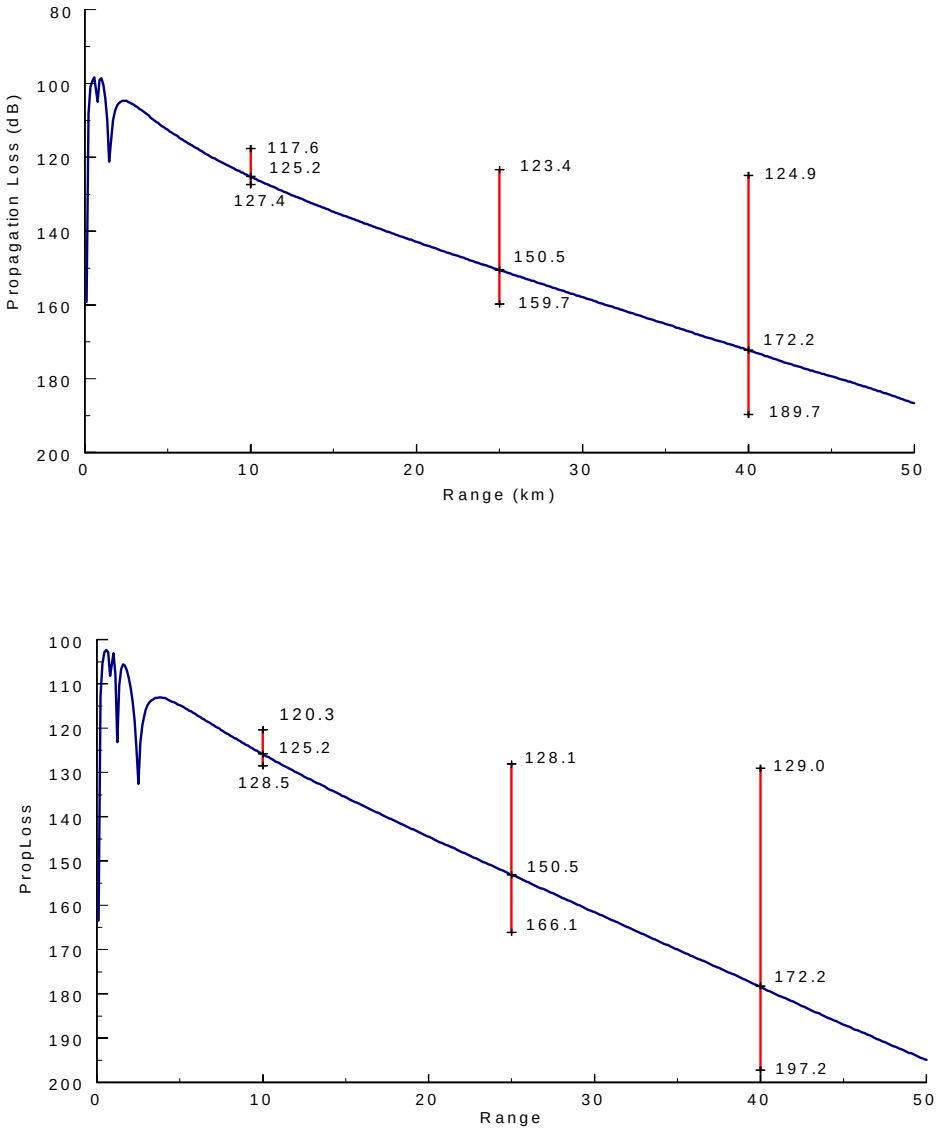

Figure 4. Propagation loss (PL) versus range at 5-m altitude for 3 and 5 GHz (top and bottom graph, respectively) transmitters at 15 m. Numbers associated with the vertical bars show minimum, standard atmosphere, and maximum PL at 10, 25, and 40 km.

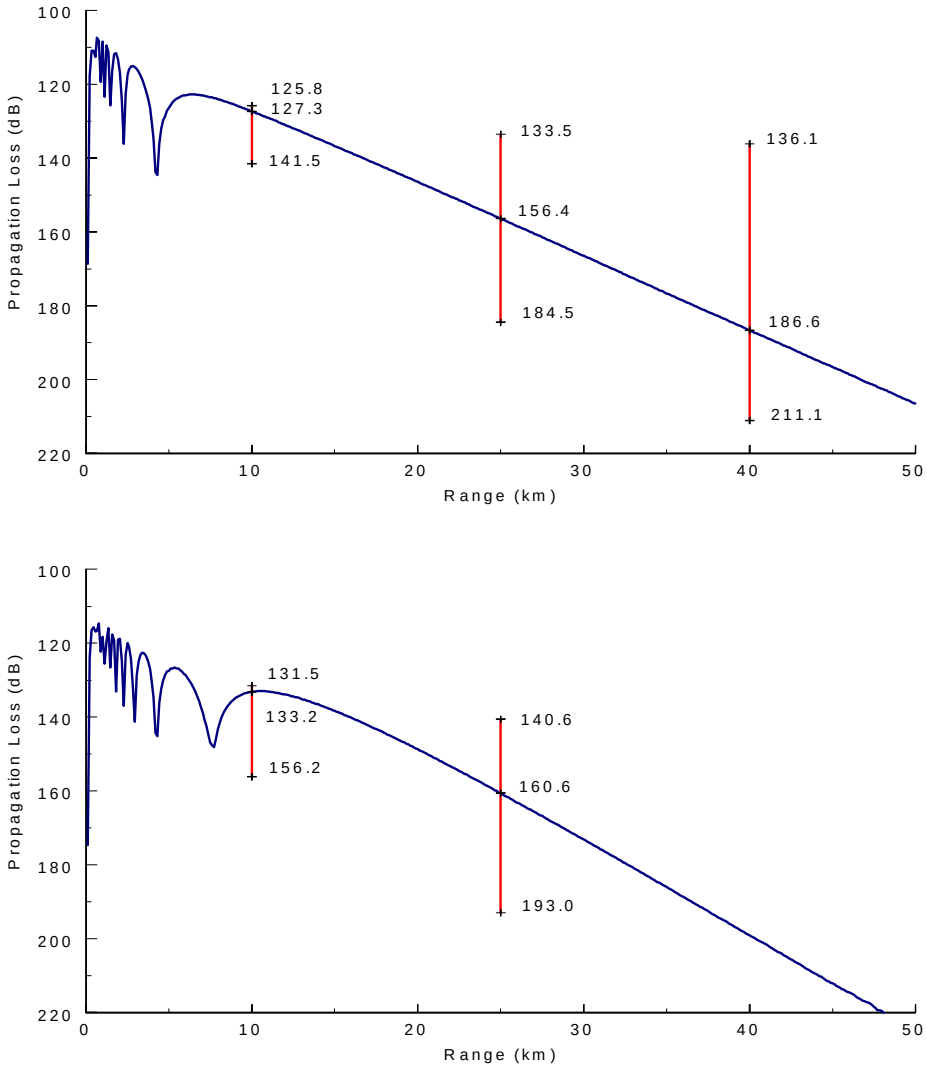

Figure 5. Propagation loss (PL) versus range at 5-m altitude for 9 and 18 GHz (top and bottom graph, respectively) transmitters at 15 m. Numbers associated with the vertical bars show minimum, standard atmosphere, and maximum PL at 10, 25, and 40 km for 9 GHz and 10 and 25 km for 18 GHz.

RESULTS

STATISTICS

For the scenarios of the four frequencies and the multiple ranges, the difference between propagation loss determined for the full stability-dependent modified refractivity profiles and propagation loss determined for the neutral-stability modified refractivity profiles was calculated. Figures 6 through 9 show histograms of the differences. The difference distributions tend to be skewed at 3 and 5 GHz, but symmetric at 9 and 18 GHz. All distributions are sharply peaked and the mean differences are near zero. Table 4 shows the descriptive statistics of the distributions for the four frequencies and multiple ranges. The mean propagation loss (PL) differences are small and the standard deviations of the differences are on the order of a few dB, indicating that the neutral profile estimate is reasonably good.

Table 4. Statistics of propagation loss (PL) differences between PL from stability-dependent profiles and PL from neutral profiles.

Frequency	Range	Largest Negative PL Difference (dB)	Largest Positive PL Difference (dB)	Mean PL Difference (dB)	Median PL Difference (dB)	Standard Deviation of PL Differences (dB)
3 GHz	10 km	-1.7	4.4	0.04	0.00	0.64
	25 km	-6.4	9.5	0.30	0.40	1.73
	40 km	-12.7	12.3	0.52	1.00	2.85
5 GHz	10 km	-4.7	1.7	-0.07	0.00	0.43
	25 km	-9.2	10.4	-0.03	0.10	1.67
	40 km	-17.6	8.4	0.26	0.40	2.86
9 GHz	10 km	-13.1	12.8	0.24	0.10	2.74
	25 km	-24.2	21.9	0.14	0.10	4.64
	40 km	-16.5	27.7	0.32	0.20	3.91
18 GHz	10 km	-17.0	18.7	-0.73	-0.10	4.84
	25 km	-18.9	19.2	0.31	0.40	4.66

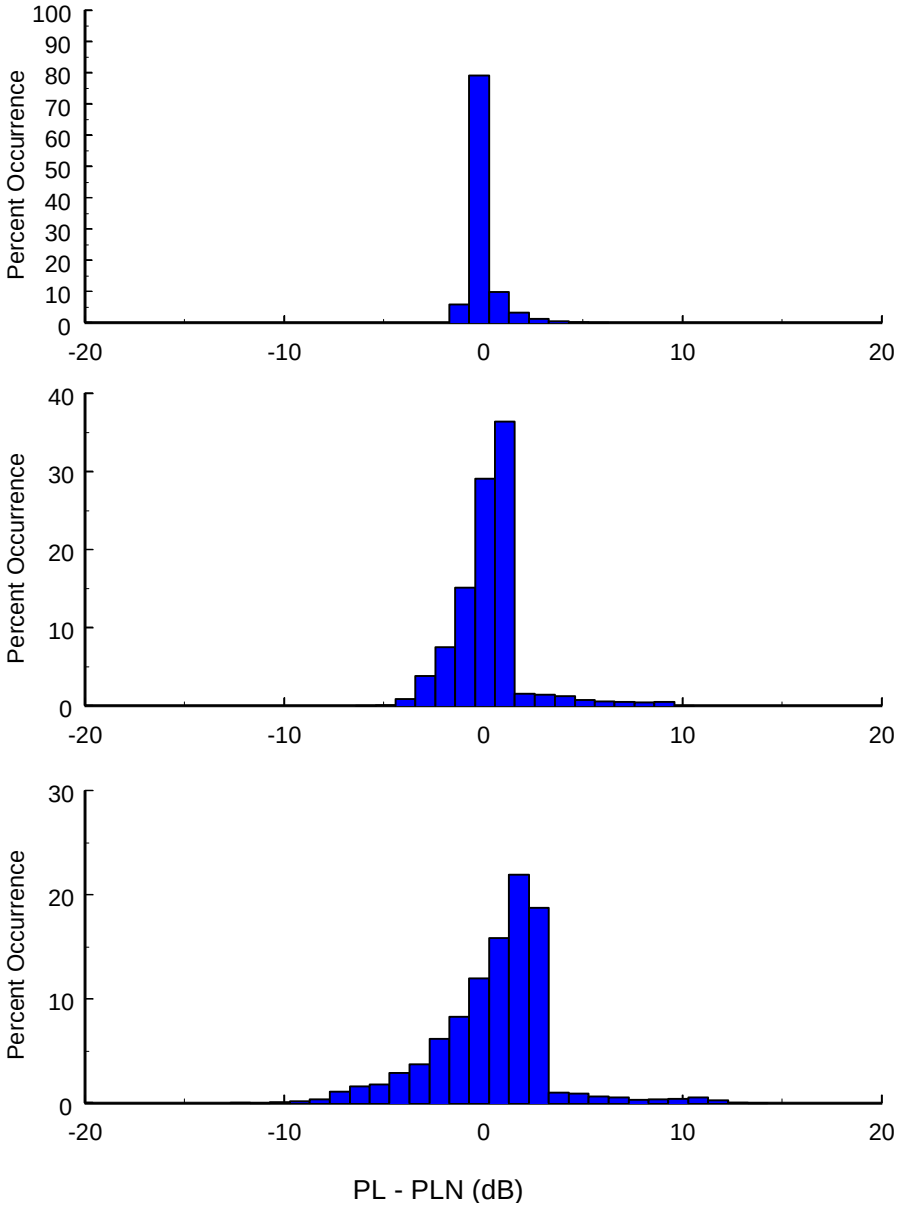

Figure 6. Histogram of differences between propagation loss for stability-dependent profiles (PL) and propagation loss for neutral profiles (PLN) at 3 GHz and ranges of 10 km (top), 25 km (middle), and 40 km (bottom).

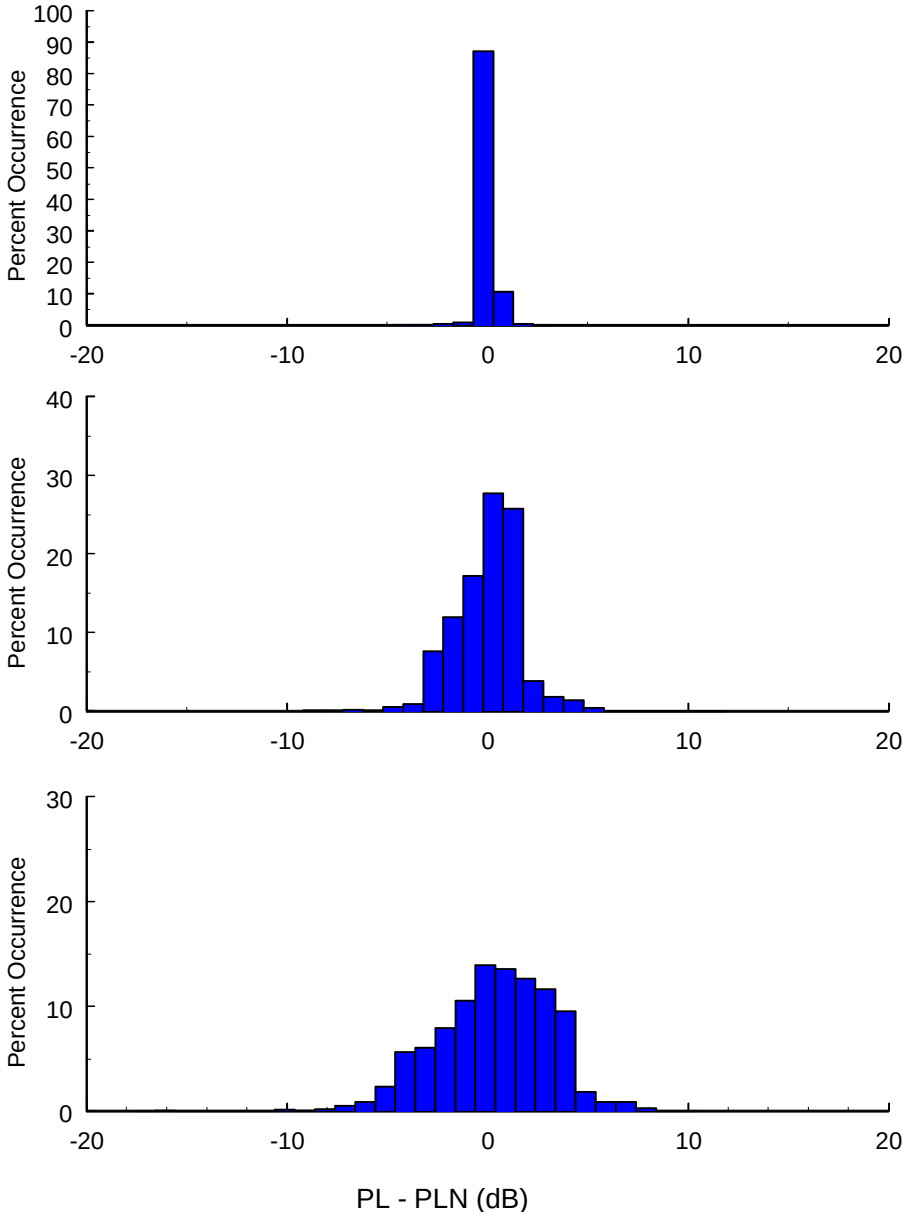

Figure 7. Histogram of differences between propagation loss for stability-dependent profiles (PL) and propagation loss for neutral profiles (PLN) at 5 GHz and ranges of 10 km (top), 25 km (middle), and 40 km (bottom).

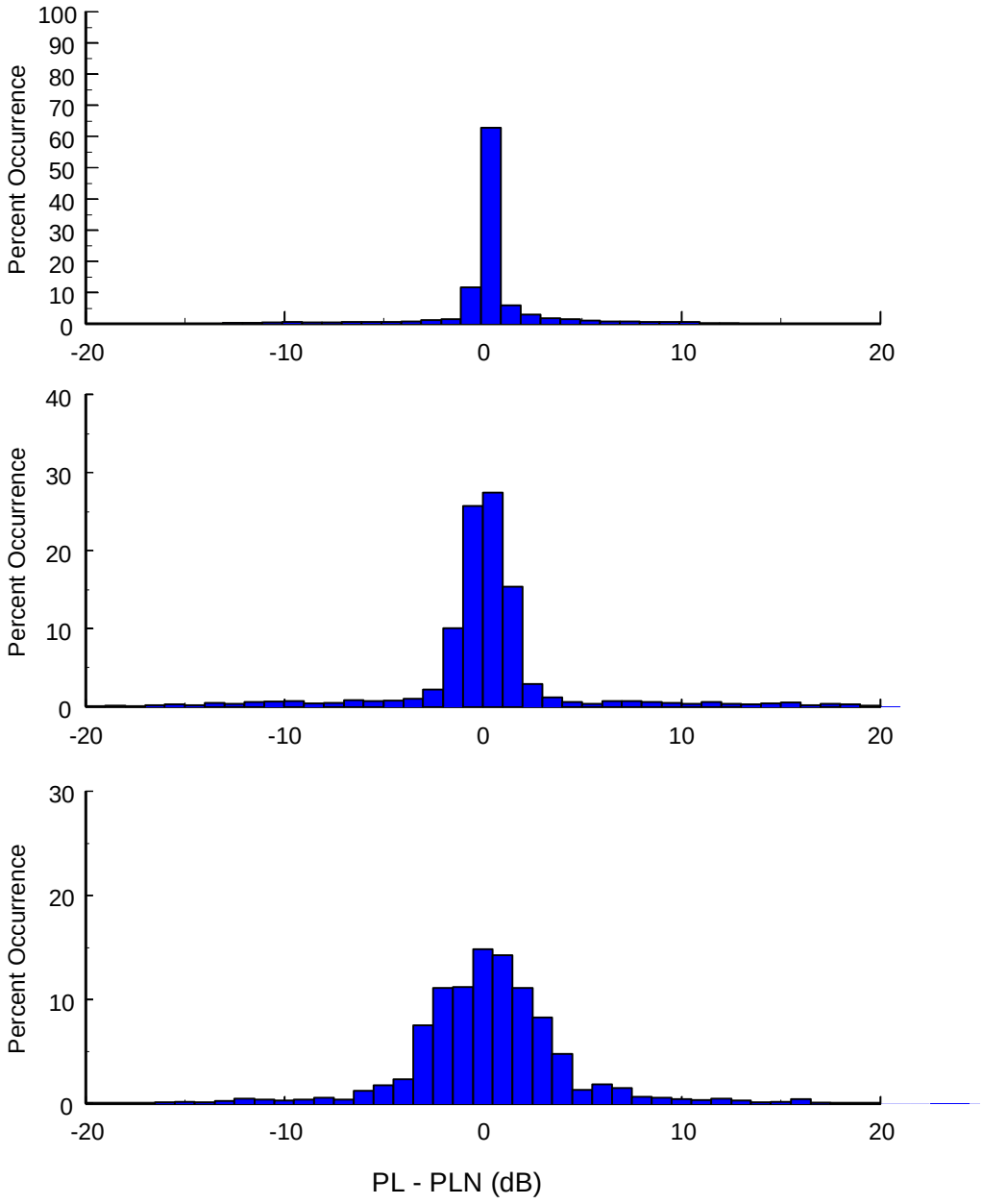

Figure 8. Histogram of differences between propagation loss for stability-dependent profiles (PL) and propagation loss for neutral profiles (PLN) at 9 GHz and ranges of 10 km (top), 25 km (middle), and 40 km (bottom).

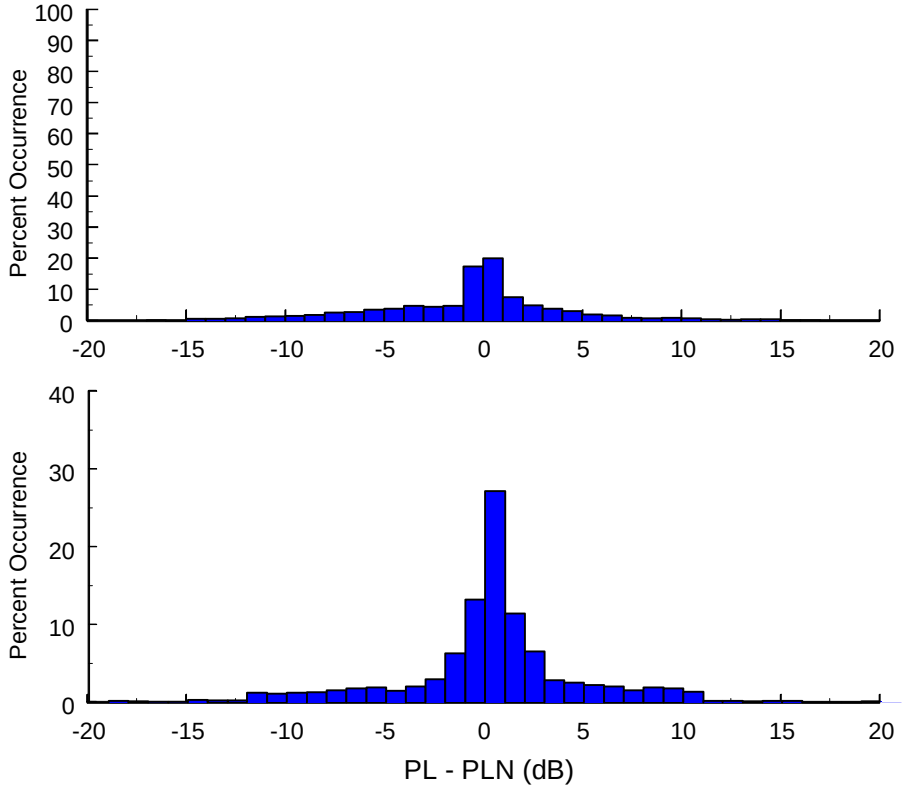

Figure 9. Histogram of differences between propagation loss for stability-dependent profiles (PL) and propagation loss for neutral profiles (PLN) at 18 GHz and ranges of 10 km (top) and 25 km (bottom).

OBSERVATIONS

Because the range of variation chosen for the bulk parameters was arbitrary, and there is no climatological data as to the joint occurrence of any given combination of parameters, it is worthwhile to examine the differences further. Figures 10 through 13 show propagation loss differences plotted versus evaporation duct height. The differences are not evenly distributed over the range of evaporation duct height. Differences tend to remain small from approximately -5 m (27-m subrefractive layer height) to approximately 15-m evaporation duct height for 3, 5, and 9 GHz and over a slightly smaller range at 18 GHz. Outside these ranges, differences increase markedly. Viewed another way, figures 14 through 17 show both PL from stability-dependent profiles and PL from neutral profiles versus evaporation duct height. At 5, 9, and 18 GHz, the variations in the plot of PL at the higher duct heights show the effects of multiple modes being propagated in the duct. There is a wider variation in resulting PL at higher duct heights. The neutral evaporation duct height at which multi-mode propagation begins to be significant is a function of frequency and has been previously estimated (Patterson et al., 1990) as shown in table 5. The duct heights of table 5 are in reasonable qualitative agreement with the increase in differences between PL from stability-dependent profiles and PL from neutral profiles shown figures 10 through 17. The impact of this increase in differences is that simulations of propagation effects parametric in evaporation duct height become less represen-

tative of real propagation effects at higher duct heights. Qualitatively, from figures 10 through 17, this also appears to be true for more negative duct heights (higher subrefractive layers). Table 5 also shows approximate subrefractive layer heights above which multi-mode propagation begins to be significant and simulation using a neutral profile becomes less representative of real propagation effects.

Table 5. Estimated neutral evaporation duct and subrefractive layer height at which multi-mode propagation begins to be significant at a given frequency.

Frequency (GHz)	Neutral Evaporation Duct Height (m)	Neutral Subrefractive Layer Height (m)
3	30	40
5	22	27
10	14	16
18	10	10

A consequence of the inverse correlation between frequency and the evaporation duct height at which multiple modes become important is that the neutral profile can be a very good approximation to the propagation effects of the full stability-dependent profile at one frequency, but not at another. Table 6 shows such an example for the propagation loss at 10 km. The differences in PL from a stability-dependent profile and a neutral profile are small at 3 and 5 GHz, but much larger at 9 and 18 GHz.

Table 7 shows the bulk parameters and evaporation duct height for the results in table 6. The evaporation duct height for this set of bulk parameters is 17.5 m. In table 5, the 17.5-m evaporation duct height falls between the values at 5 GHz and 10 GHz. This height would indicate that 3 and 5 GHz should be dominated by single-mode propagation and that 9 and 18 GHz should be affected by multiple modes propagating in the duct. Thus, we should expect that the neutral profile would be a good approximation of the stability-dependent profile propagation loss at the two lower frequencies, but not as good at the two higher frequencies.

Table 6. Propagation loss from stability-dependent profile (PL), neutral profile (PLN), and the difference (PL-PLN) versus frequency.

Frequency (GHz)	PL (dB)	PLN (dB)	PL Difference (dB)
3	119.6	120.9	-1.3
5	121.1	121.6	-0.5
9	141.5	128.7	12.8
18	143.4	132.1	11.3

Table 7. Bulk parameters that describe evaporation duct profile that provided PL values of table 6.

Wind Speed (m/s)	Air Temp (°C)	Sea Temp (°C)	Relative Humidity (%)	Evaporation Duct Height (m)
7.5	27	30	60	17.5

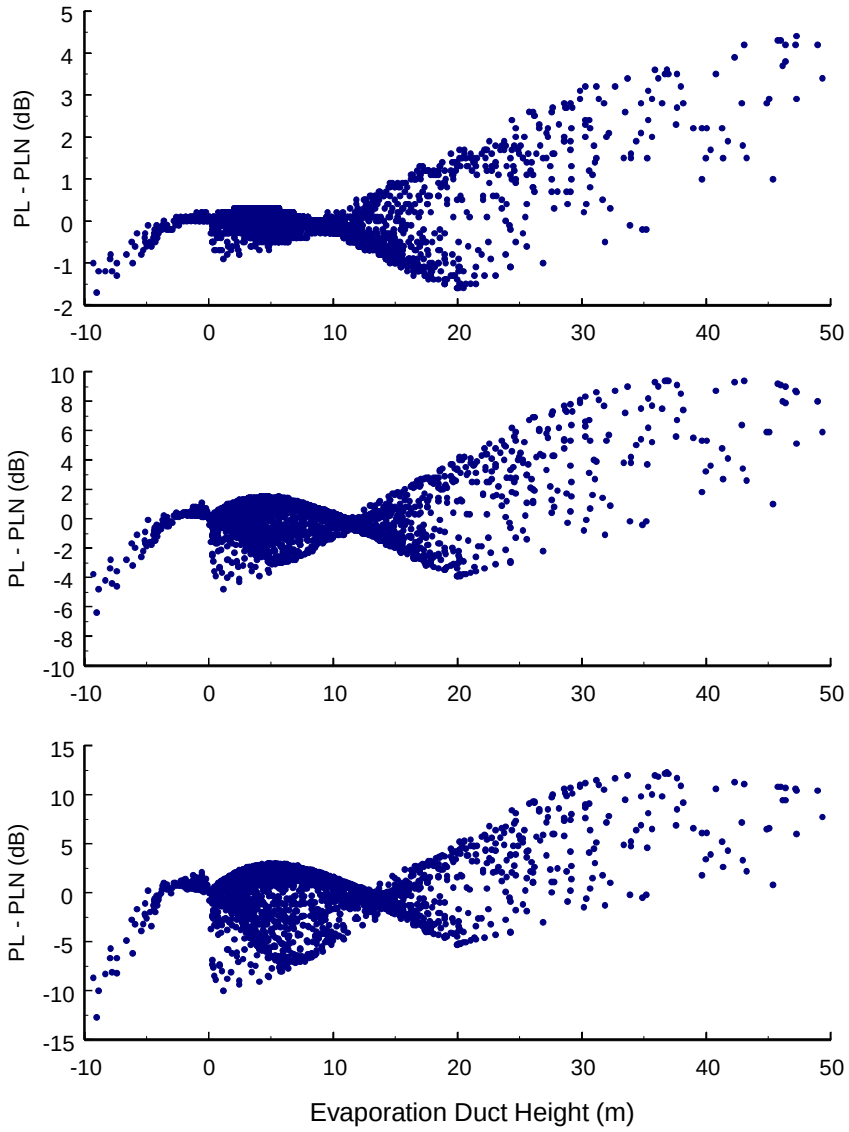

Figure 10. Differences between propagation loss for stability-dependent profiles (PL) and propagation loss for neutral profiles (PLN) versus evaporation duct height at 3 GHz and ranges of 10 km (top), 25 km (middle), and 40 km (bottom).

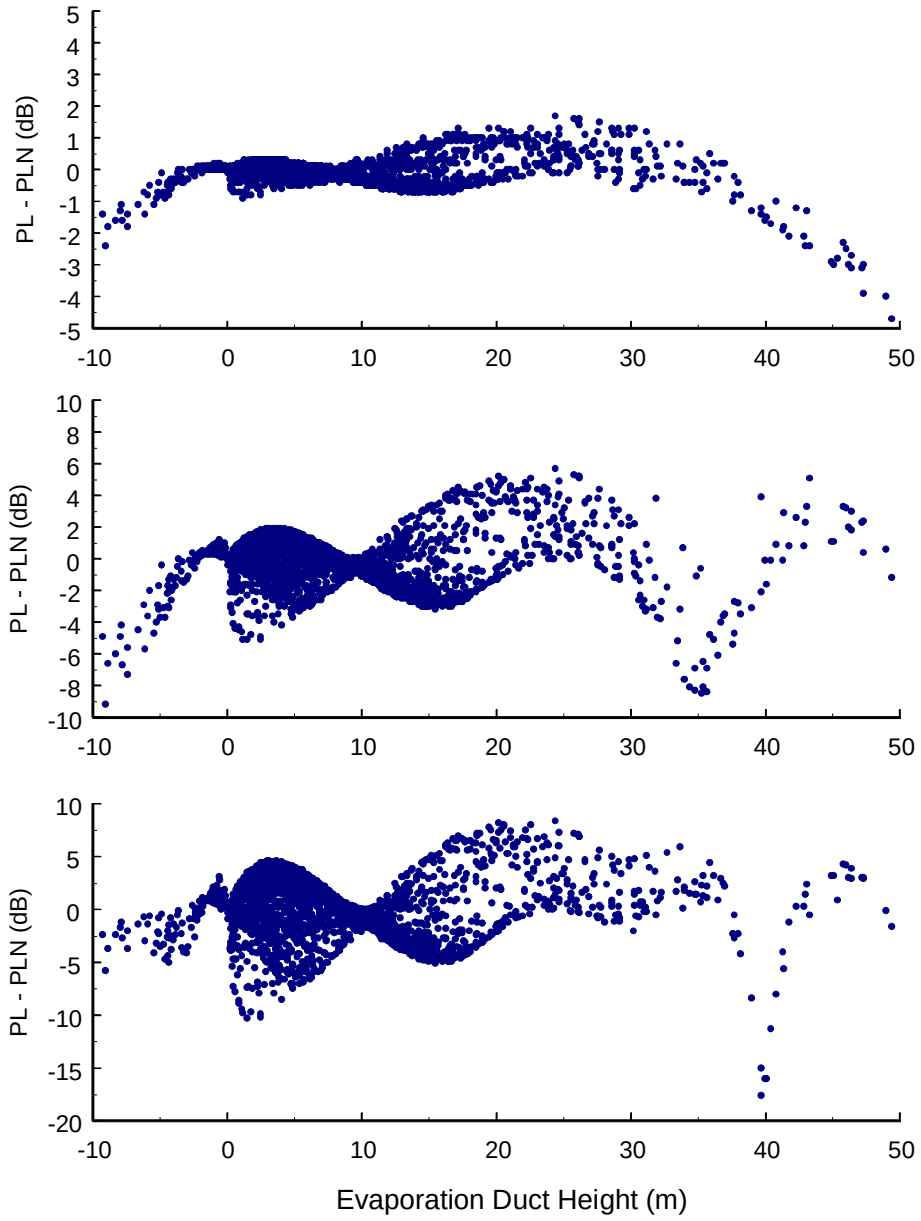

Figure 11. Differences between propagation loss for stability-dependent profiles (PL) and propagation loss for neutral profiles (PLN) versus evaporation duct height at 5 GHz and ranges of 10 km (top), 25 km (middle), and 40 km (bottom).

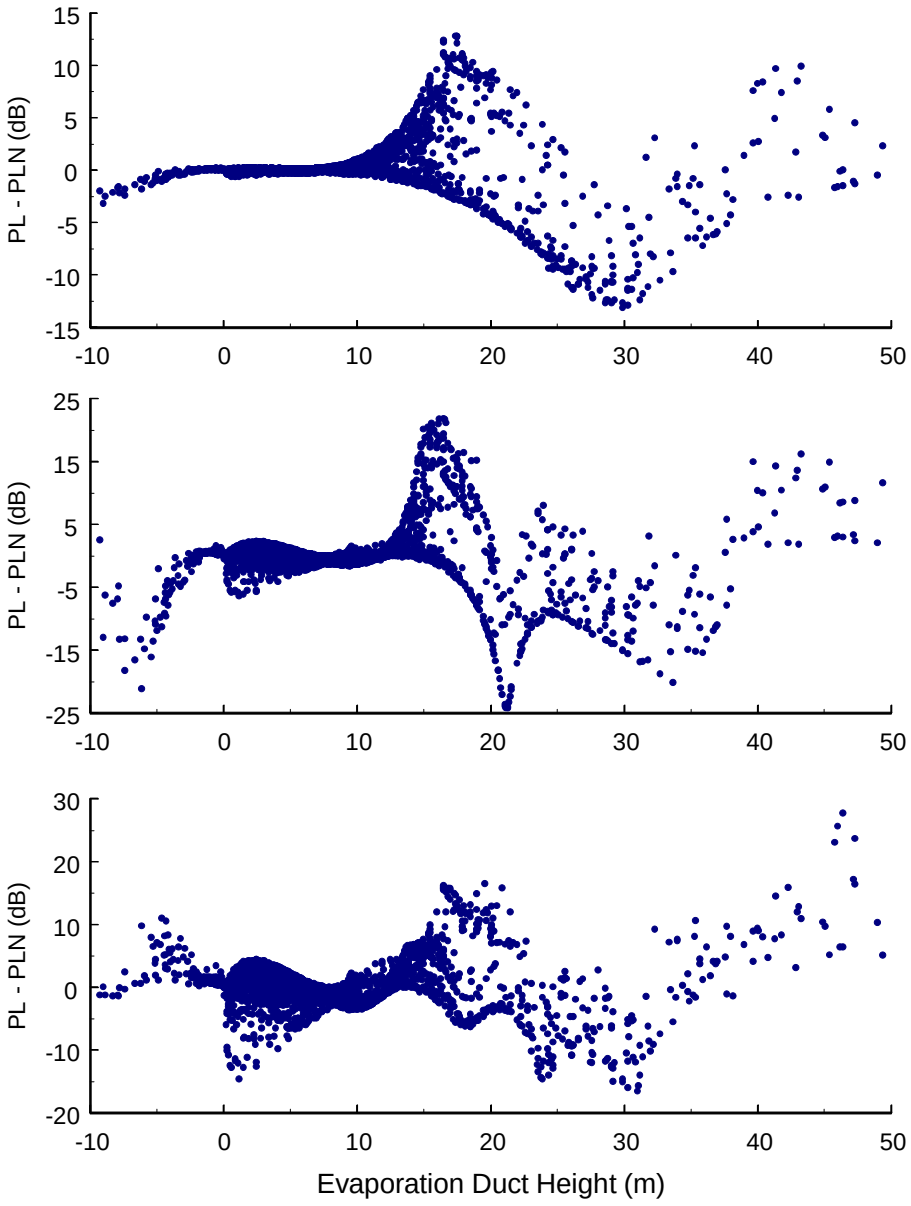

Figure 12. Differences between propagation loss for stability-dependent profiles (PL) and propagation loss for neutral profiles (PLN) versus evaporation duct height at 9 GHz and ranges of 10 km (top), 25 km (middle), and 40 km (bottom).

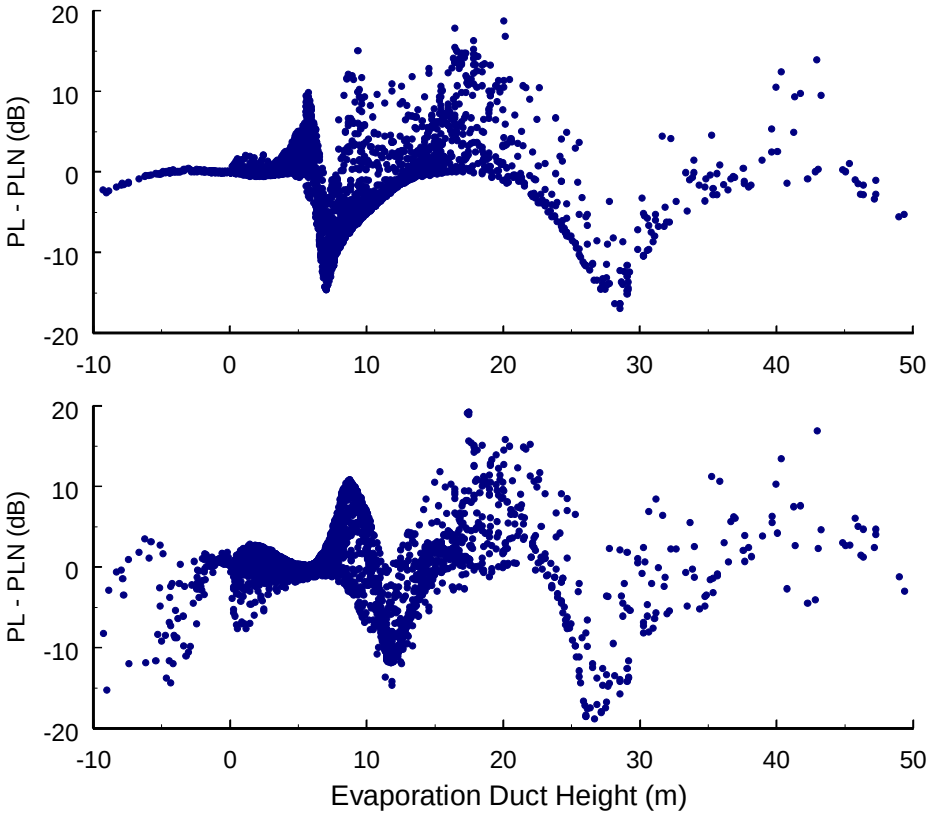

Figure 13. Differences between propagation loss for stability-dependent profiles (PL) and propagation loss for neutral profiles (PLN) versus evaporation duct height at 18 GHz and ranges of 10 km (top) and 25 km (bottom).

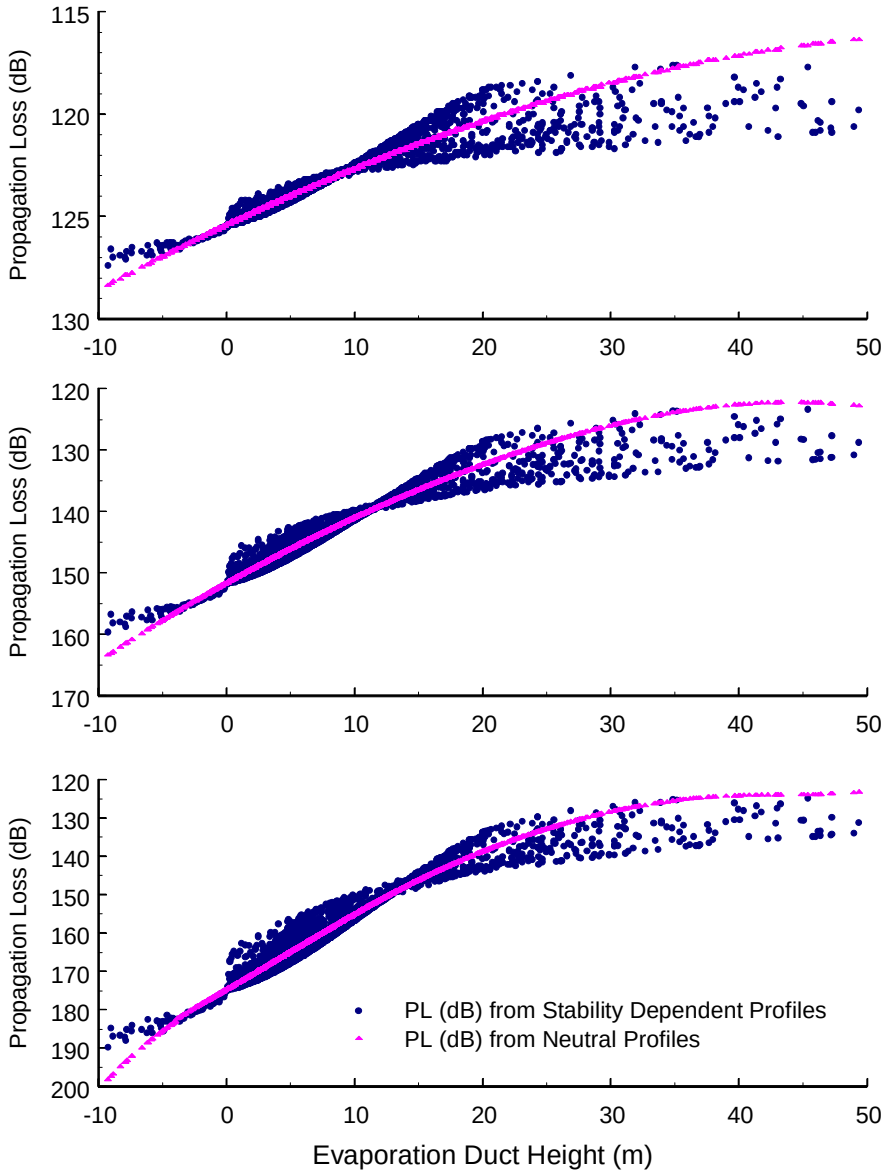

Figure 14. Overplot of propagation loss for stability-dependent profiles and propagation loss for neutral profiles versus evaporation duct height at 3 GHz and ranges of 10 km (top), 25 km (middle), and 40 km (bottom).

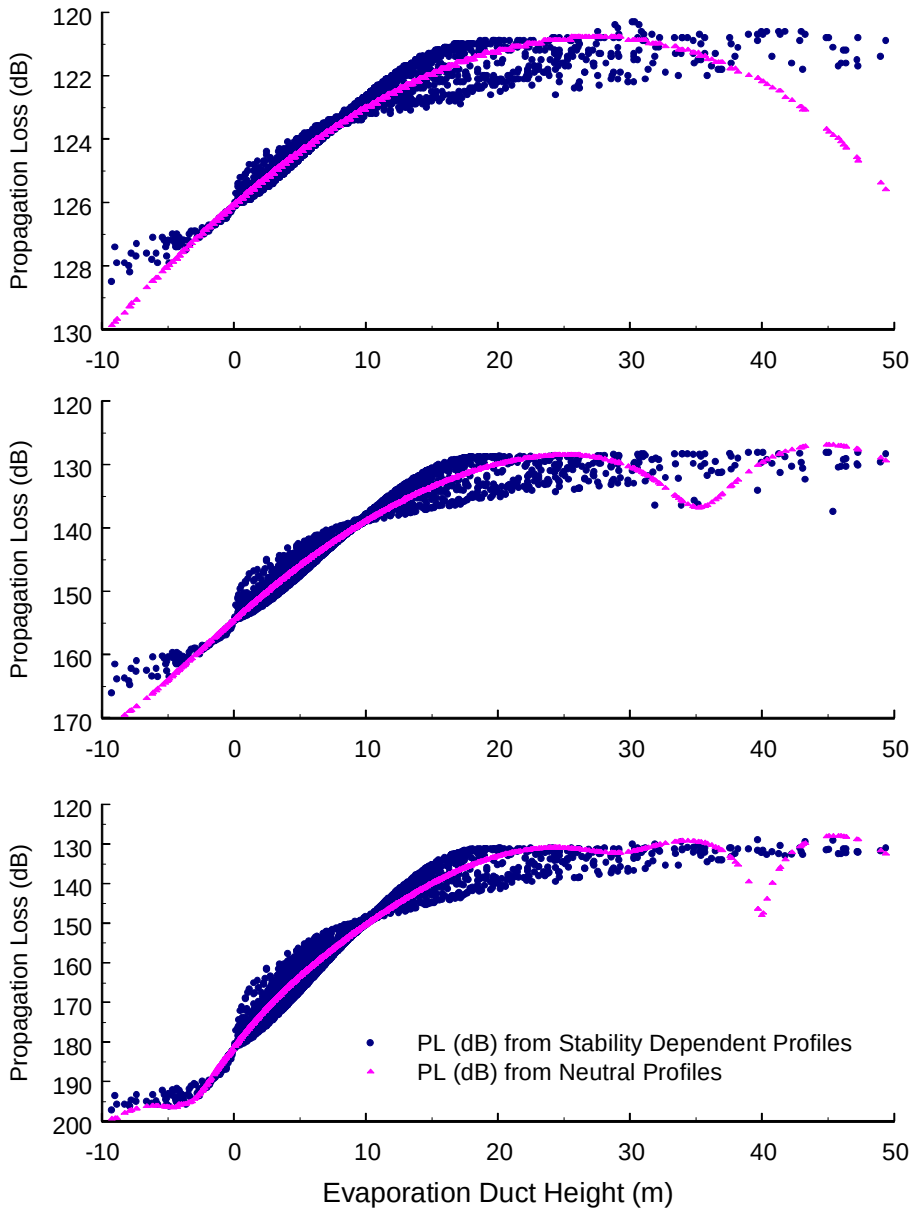

Figure 15. Overplot of propagation loss for stability-dependent profiles and propagation loss for neutral profiles versus evaporation duct height at 5 GHz and ranges of 10 km (top), 25 km (middle), and 40 km (bottom).

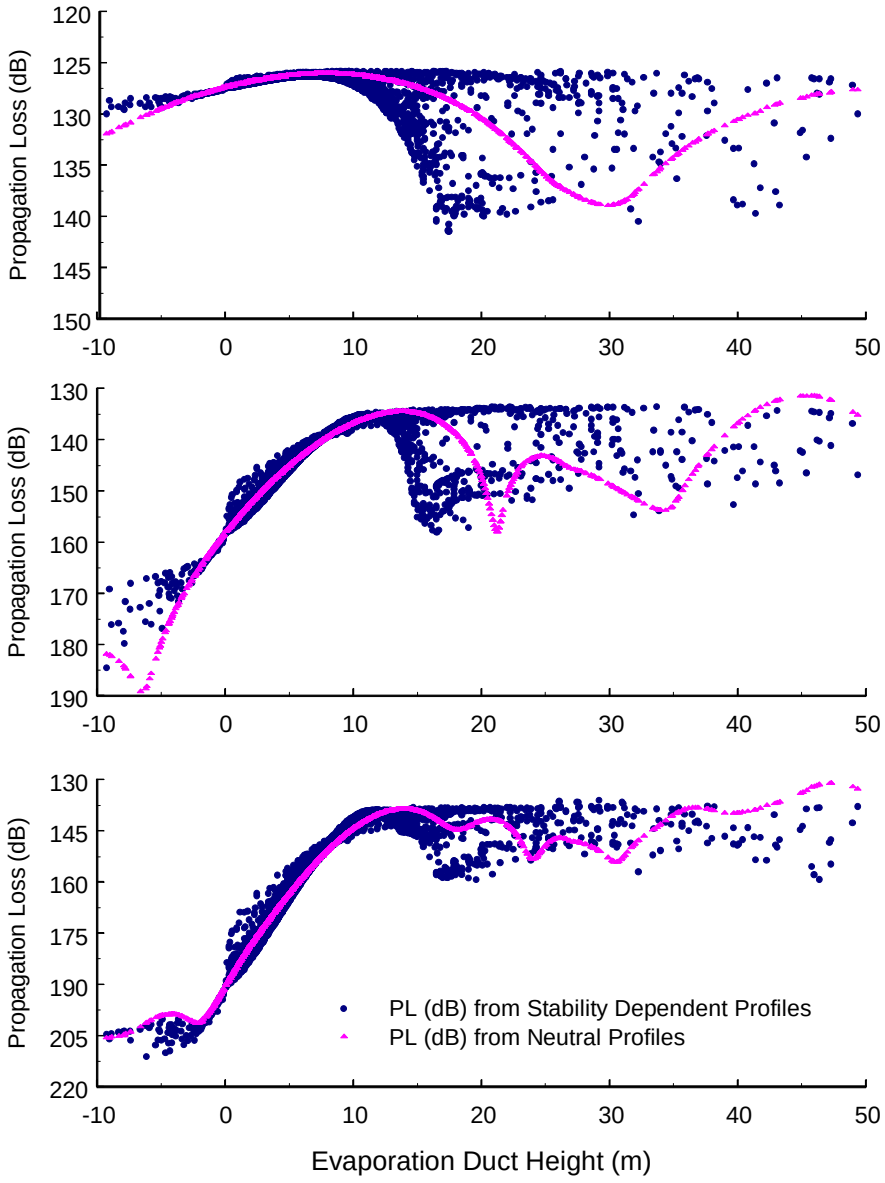

Figure 16. Overplot of propagation loss for stability-dependent profiles and propagation loss for neutral profiles versus evaporation duct height at 9 GHz and ranges of 10 km (top), 25 km (middle), and 40 km (bottom).

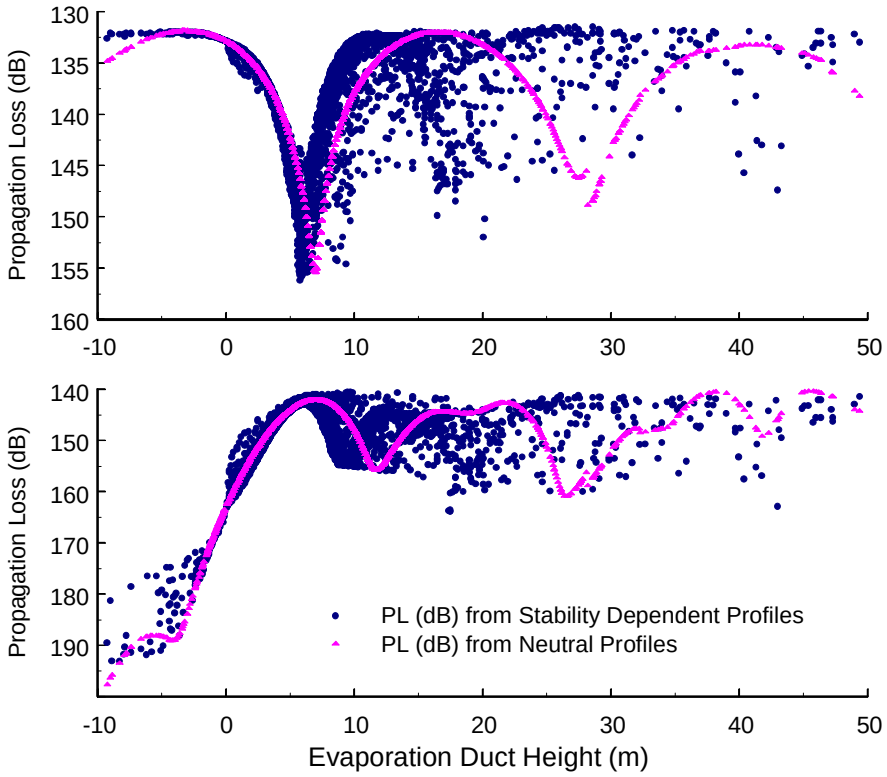

Figure 17. Overplot of propagation loss for stability-dependent profiles and propagation loss for neutral profiles versus evaporation duct height at 18 GHz and ranges of 10 km (top) and 25 km (bottom).

Figures 18 to 21 show the difference in propagation loss from stability-dependent and neutral modified refractivity profiles versus the stability parameter, z/L, for the four frequencies and multiple ranges. While there are relatively large differences in PL in the unstable and stable regions, most of the larger differences occur near neutral. This occurrence is consistent with figure 3, which showed that the higher duct and subrefractive layer heights occurred near neutral. Therefore, because the higher duct and subrefractive layer heights support multi-mode propagation, we conclude that the largest PL differences will also occur in near-neutral conditions.

Note that the propagation effects of a 0-m evaporation duct are not the same as a standard atmosphere. A close comparison of the standard atmosphere PL values from figures 4 and 5 with the 0-m duct height values in figures 14 through 17 shows that 0-m evaporation duct PL values may be up to a few dB greater than standard atmosphere, particularly at 25 and 40 km. This increase is the result of the standard atmosphere gradient being 0.118 *M*/m versus the 0-m evaporation duct gradient of 0.130 *M*/m, determined by the derivative of equation (10).

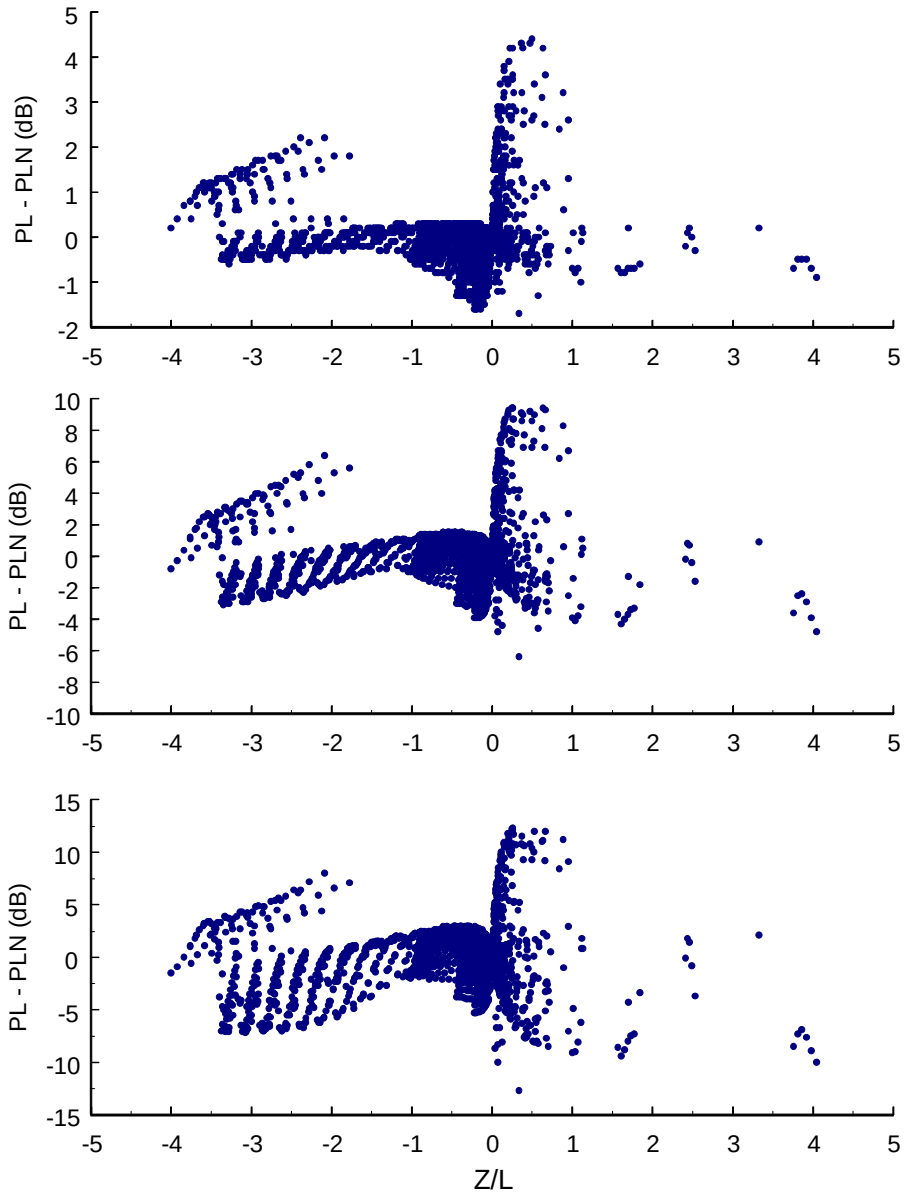

Figure 18. Differences between propagation loss for stability dependent profiles (PL) and propagation loss for neutral profiles (PLN) versus the stability parameter, z/L, at 3 GHz and ranges of 10 km (top), 25 km (middle), and 40 km (bottom).

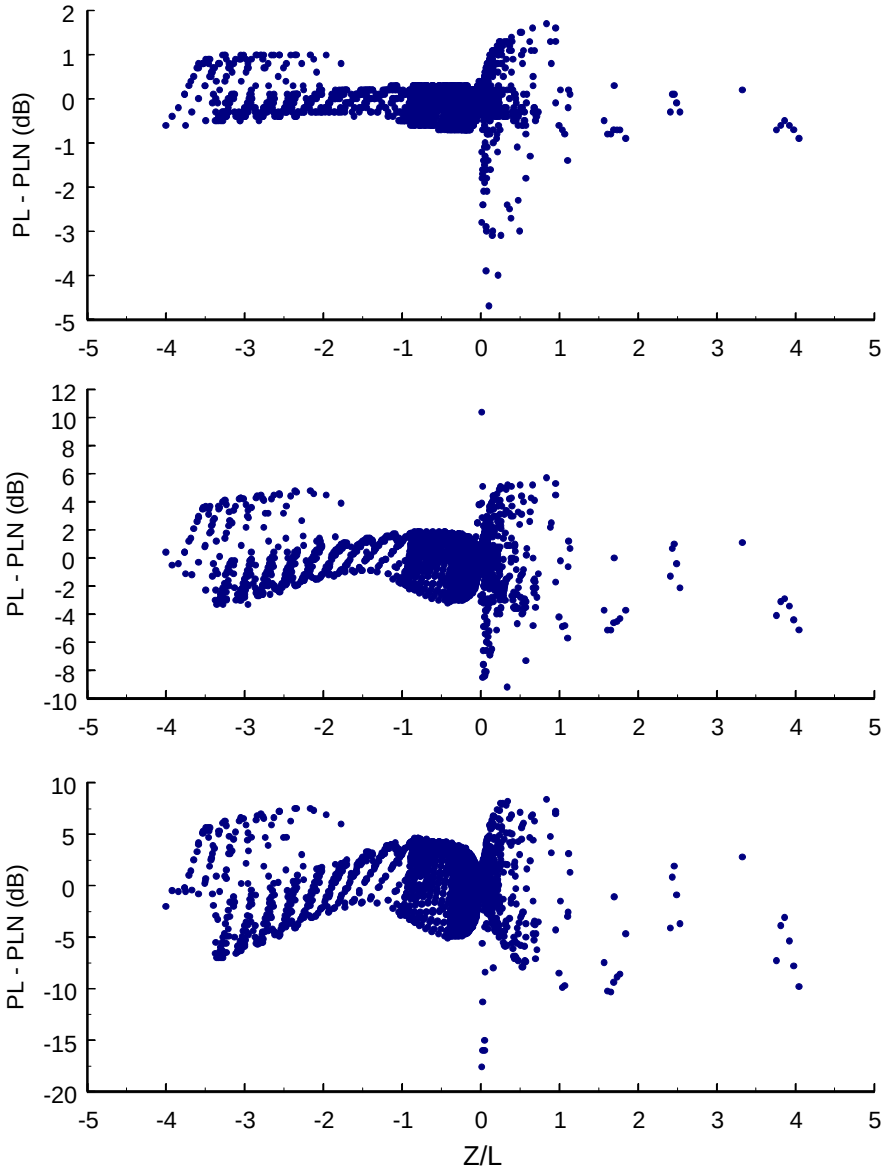

Figure 19. Differences between propagation loss for stability-dependent profiles (PL) and propagation loss for neutral profiles (PLN) versus the stability parameter, z/L, at 5 GHz and ranges of 10 km (top), 25 km (middle), and 40 km (bottom).

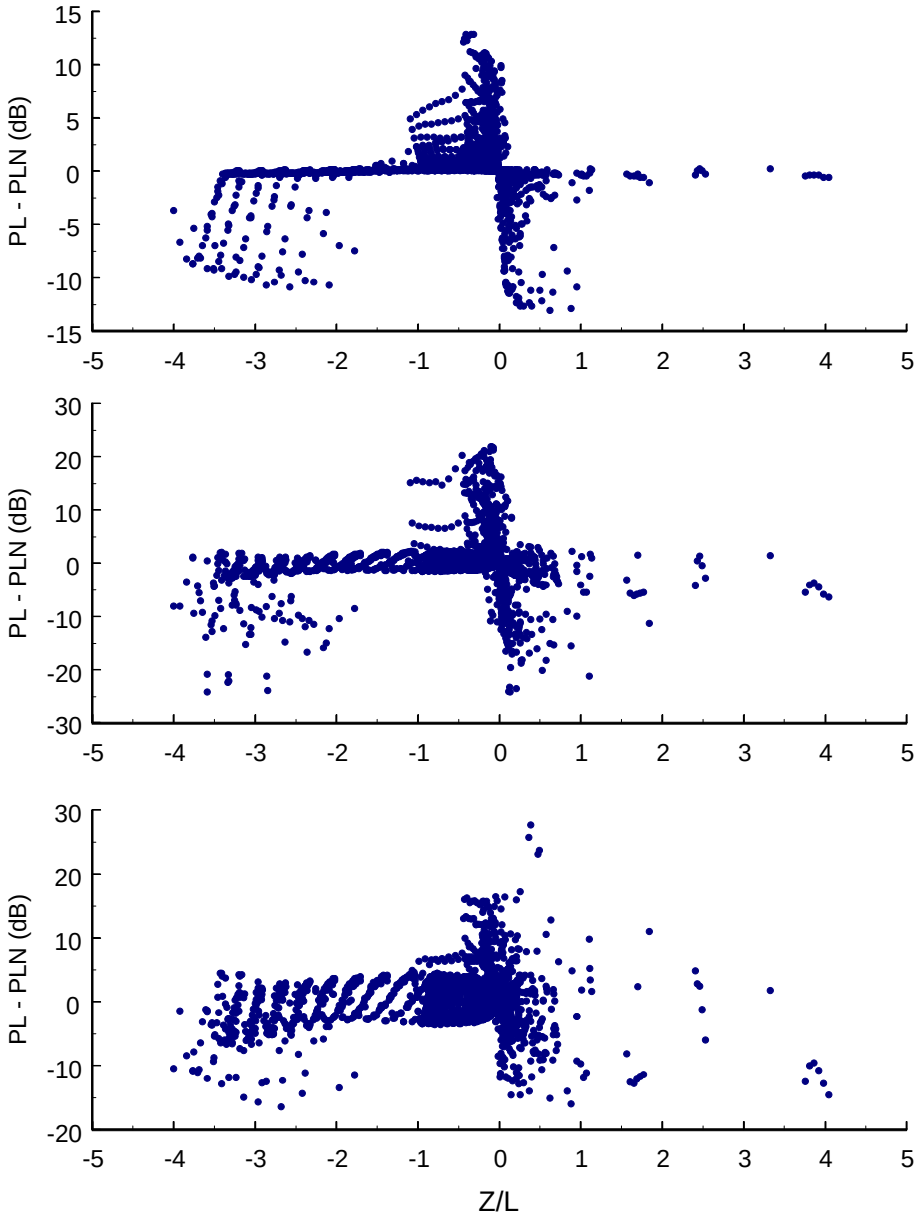

Figure 20. Differences between propagation loss for stability-dependent profiles (PL) and propagation loss for neutral profiles (PLN) versus the stability parameter, z/L, at 9 GHz and ranges of 10 km (top), 25 km (middle), and 40 km (bottom).

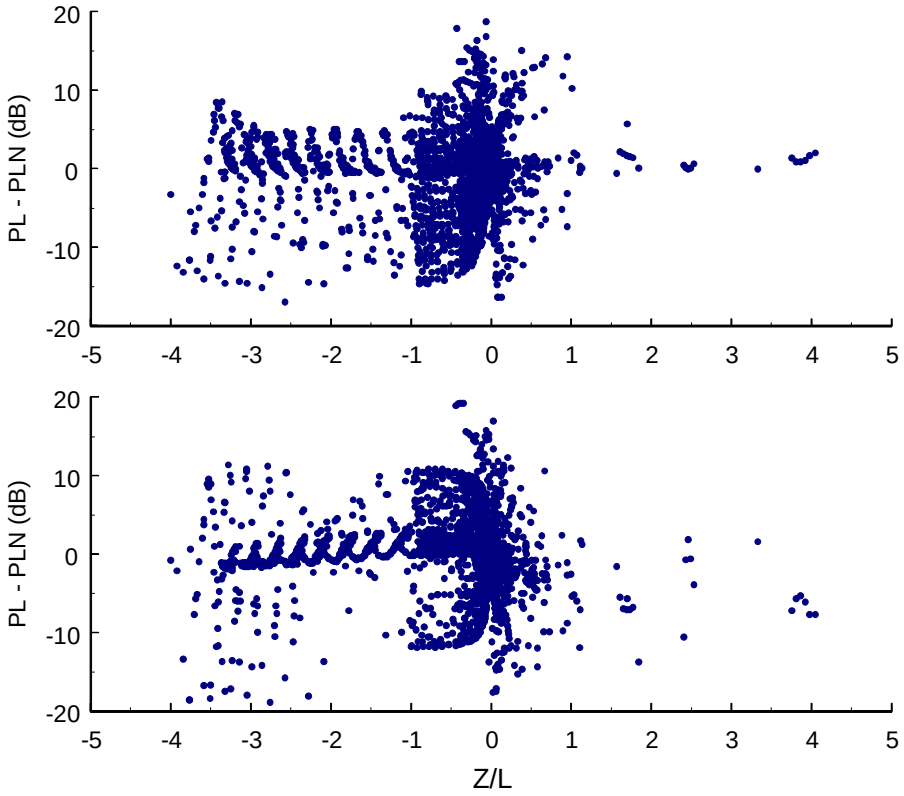

Figure 21. Differences between propagation loss for stability-dependent profiles (PL) and propagation loss for neutral profiles (PLN) versus the stability parameter, z/L, at 18 GHz and ranges of 10 km (top) and 25 km.

CONCLUSIONS

This study finds that subrefractive profiles in the atmospheric surface layer can be parameterized by a characteristic height similar to the evaporation duct height. This parameter can be in terms of subrefractive layer height or negative evaporation duct height. Equation (13) relates the two heights. The parameter "subrefractive layer height" is an easily understood concept and is related to a physical feature of the refractivity profile. The parameter "negative evaporation duct height" is not related to a physical feature of the refractivity profile and evaporation is not the surface layer physical process involved in subrefraction, rather condensation is occurring. However, using a negative duct height allows plotting of propagation loss predictions versus one parameter demonstrated here.

This study demonstrates that using neutral-stability refractivity profiles, equation (10) or (12), yields a good approximation of the propagation loss resulting from using full stability-dependent profiles over a typical range of bulk meteorological parameters. The accuracy of this approximation degrades as the refractive profile supports the propagation of multiple modes, *i.e.*, as the duct height increases. This phenomena occurs for higher evaporation duct heights. Table 5 presents the approximate duct heights at which multiple-mode propagation becomes significant.

REFERENCES

Anderson, K. D. 1987. "Worldwide Distributions of Shipboard Surface Meteorological Observations for EM Propagation Analysis." NOSC Technical Document 1150 (Sep). Naval Ocean Systems Center*, San Diego, CA.

Anderson, K. D. 1995. "Radar Detection of Low-Altitude Targets in a Maritime Environment." *IEEE Transactions on Antennas and Propagation*, vol. 43, no. 6 (Jun), pp.609–613.

Bean, B. R. and E. J. Dutton. 1968. *Radio Meteorology*, Dover Publications, New York, NY.

Blanc, T. V. 1987. "Accuracy of Bulk-Method-Determined Flux, Stability, and Sea Roughness," *Journal of Geophysical Research*, vol. 92, no. C4, pp. 3867–3876.

Dockery, G. D. 1987. "Description and Validation of the Electromagnetic Parabolic Equation Propagation Model (EMPE)," FS-87-152 (Sep). Johns Hopkins University/Applied Physics Laboratory, Laurel, MD.

Frederickson, P. A., K. L. Davidson, and A. K. Goroch. 2000. "Operational Bulk Evaporation Duct Model for MORIAH," Draft version 1.2, NPS Report 2000.

Gossard, E. E. and R. G. Strauch. 1983. Radar Observation of Clear Air and Clouds, Elsevier, New York, NY.

Hitney, H. V. and R. Vieth. 1990. "Statistical Assessment of Evaporation Duct Propagation," *IEEE Transactions on Antennas and Propagation*, vol. 38, no. 6 (Jun), pp. 794–799.

Hitney, H. V. and L. R. Hitney. 1990. "Frequency Diversity Effects of Evaporation Duct Propagation," *IEEE Transactions on Antennas and Propagation*, vol. 38, no.10 (Oct), pp. 1694–1700.

Hitney, H. V. 1992. "Hybrid Ray Optics and Parabolic Equation Methods for Radar Propagation Modeling," *IEE International Conference: RADAR '92*, *Conference Publication No. 365*, (pp. 58-61). 12–13 October 1992, Brighton, UK.

Hsu, S. A. 1992. "An Overwater Stability Criterion for the Offshore and Coastal Dispersion Model," *Boundary Layer Meteorology*, vol. 50, pp. 397–402.

Jeske, H. 1973. "State and Limits of Prediction Methods of Radar Wave Propagation Conditions Over Sea." In *Modern Topics in Microwave Propagation and Air–Sea Interaction*, p. 131–148, A. Zancla, Ed. Reidel Publishers, Boston, MA.

Panofsky, H. A. and J. A. Dutton. 1984. *Atmospheric Turbulence: Models and Methods for Engineering Applications*. Wiley, New York, NY.

Patterson, W. L. 1987. "Historical Electromagnetic Propagation Condition Database Description," NOSC* Technical Document 1149 (Sep). Naval Ocean Systems Center, San Diego, CA.

* now SSC San Diego

Patterson, W. L., C. P. Hattan, H. V. Hitney, R. A. Paulus, A. E. Barrios, G. E. Lindem, and K. D. Anderson. 1990. "Engineer's Refractive Effects Prediction System (EREPS) Revision 2.0." NOSC* Technical Document 1342 (Feb), Naval Ocean Systems Center, San Diego, CA.

Paulus, R. A. 1989. "Specification for Evaporation Duct Height Calculations," NOSC* Technical Document 1596 (Jul), Naval Ocean Systems Center, San Diego, CA.

Paulus, R. A. and K. D. Anderson. 2000. "Application Of An Evaporation Duct Climatology in the Littoral," Proceedings of Battlespace Atmospheric and Cloud Impact on Military Operations (BACIMO) 2000 Conference, 25–27 April, Ft. Collins, CO.

U.S. Navy. 1974. *U.S. Navy Marine Climatic Atlas of the World*, series, Commander, Naval Weather Service Command, U.S. Government Printing Office, Washington, D.C.

* now SSC San Diego

REPORT DOCUMENTATION PAGE

Form Approved
OMB No. 0704-01-0188

PLEASE DO NOT RETURN YOUR FORM TO THE ABOVE ADDRESS.

1. REPORT DATE *(DD-MM-YYYY)*	2. REPORT TYPE	3. DATES COVERED *(From - To)*
11-2000	Technical	

4. TITLE AND SUBTITLE
PARMETRIC STUDY OF PROPAGATION IN EVAPORATION DUCTING AND SUBREFRACTIVE CONDITIONS

5a. CONTRACT NUMBER

5b. GRANT NUMBER

5c. PROGRAM ELEMENT NUMBER
PE0602435N

6. AUTHORS
R. A. Paulus

5d. PROJECT NUMBER

5e. TASK NUMBER
DN302216

5f. WORK UNIT NUMBER
MPB3

7. PERFORMING ORGANIZATION NAME(S) AND ADDRESS(ES)
SSC San Diego
San Diego, CA 92152-5001

8. PERFORMING ORGANIZATION REPORT NUMBER
TR 1844

9. SPONSORING/MONITORING AGENCY NAME(S) AND ADDRESS(ES)
Office of Naval Research (ONR 322)
800 North Quincy Street
Arlington, VA 22217-5660

10. SPONSOR/MONITOR'S ACRONYM(S)
ONR

11. SPONSOR/MONITOR'S REPORT NUMBER(S)

12. DISTRIBUTION/AVAILABILITY STATEMENT
Distribution is unlimited; public release

13. SUPPLEMENTARY NOTES

14. ABSTRACT
This report quantifies propagation loss differences that result from approximating the full stability-dependent refractivity profiles with neutral-stability profiles parameterized by duct height. It also develops a parameterization for subrefractive profiles and quantifies the propagation loss differences that result from approximating the full stability-dependent refractivity profiles with neutral-stability profiles parameterized by subrefractive layer height.

15. SUBJECT TERMS
Mission Area: Command, Control, Communications
atmospheric physics; environmental data; refractivity; evaporation duct; propagation assessment; meteorology; subrefraction

16. SECURITY CLASSIFICATION OF:			17. LIMITATION OF ABSTRACT	18. NUMBER OF PAGES	19a. NAME OF RESPONSIBLE PERSON
a. REPORT	b. ABSTRACT	c. THIS PAGE			R. A. Paulus
U	U	U	UU	86	19B. TELEPHONE NUMBER *(Include area code)* (619) 553-1424

INITIAL DISTRIBUTION

D0012	Patent Counsel	(1)
D0271	Archive/Stock	(6)
D0274	Library	(2)
D027	M. E. Cathcart	(1)
D0271	D. Richter	(1)
D858	R. A. Paulus	(1)

Defense Technical Information Center
Fort Belvoir, VA 22060–6218 (4)

SSC San Diego Liaison Office
Arlington, VA 22202–4804

Center for Naval Analyses
Alexandria, VA 22302–0268

Office of Naval Research
Attn: NARDIC (Code 362)
Arlington, VA 22217–5660

Government-Industry Data Exchange
Program Operations Center
Corona, CA 91718–8000

Office of Naval Research
Arlington, VA 22217–5660

Naval Surface Warfare Center
Dahlgren Division
Dahlgren, VA 22448–5100

Naval Postgraduate School
Meteorology Department
Monterey, CA 93943–5114

Defence Research Establishment Valcartier (DREV)
Val Belair, Quebec, G3J 1X5 Canada

Raytheon Electronic Systems
Sudbury, MA 01776

Johns Hopkins University
Applied Physics Laboratory
Laurel, MD 20723–6099